International Journal of Biological Macromolecules 283 (2024) 137659

Contents lists available at ScienceDirect

International Journal of Biological Macromolecules

journal homepage: www.elsevier.com/locate/ijbiomac

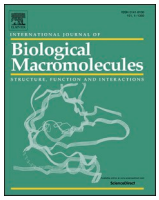

Amphiphilic pH-responsive core-shell nanoparticles can increase the performances of cellulose-based drug delivery systems

Elisa Lacroce [a], Giuseppe Nunziata [a], Francesca Cianniello [a], Emanuele Limiti [b,c], Alberto Rainer [d,e], Francesco Briatico Vangosa [a], Alessandro Sacchetti [a], Mattia Sponchioni [a], Filippo Rossi [a,*]

[a] Department of Chemistry, Materials and Chemical Engineering "Giulio Natta", Politecnico di Milano, Piazza Leonardo da Vinci 32, 20133 Milan, Italy
[b] Deptartment of Science and Technology for Sustainable Development and One Health, Università Campus Bio-Medico di Roma, via Álvaro del Portillo 21, 00128 Rome, Italy
[c] Institute of Nanotechnology (NANOTEC), National Research Council, via Monteroni, 73100 Lecce, Italy
[d] Department of Engineering, Università Campus Bio-Medico di Roma, via Álvaro del Portillo 21, 00128 Rome, Italy
[e] Fondazione Policlinico Universitario Campus Bio-Medico, via Álvaro del Portillo 200, 00128 Rome, Italy

ARTICLE INFO

Keywords:
Colloids
Drug delivery
Nanoparticles
Polymers
pH-responsive

ABSTRACT

Polymer and nanoparticles (NPs) together are able to form nanocomposite materials that combine the beneficial properties of the traditional single systems. In this work, we propose a stimuli-responsive nanocomposite system which combines pH-responsive NPs with cellulose. Ring opening polymerization (ROP) followed by two reversible addition-fragmentation chain transfer (RAFT) polymerization steps were performed to synthetize ((PHEMA-*graft*-LA_{12})-*co*-PMAA)-b-PDEGMA copolymer characterized by tailored molecular weights and low polydispersity values. Uniform NPs were obtained by nanoprecipitation of the so-obtained copolymer in water. Moreover, drug release studies (using rhodamine b, fluorescein isothiocyanate, pyrene and 5-fluorouracil) at different pHs demonstrated the pH-responsivity of NPs, revealing a significant improvement of hydrophobic molecules release at acidic conditions. In vitro tests verified the biocompatibility of NPs and the efficacy in decreasing cancer cell viability. Finally, NPs were loaded into hydroxypropylmethyl-cellulose-C_{12} matrix to obtain the final polymer-NPs composite system. The composite systems showed the ability to sustain the release of low steric hindrance drugs loaded with NPs and high steric hindrance ones loaded within the polymeric network. Overall, the proposed pH-responsive drug delivery system represents a co-delivery device which could be applied for localized treatment in different combined therapeutic program.

1. Introduction

The last decades have witnessed an increasing development of drug delivery systems (DDS), with hydrogels representing one of the most relevant material classes [1–4]. Particularly interesting are those hydrogels able to undergo sol-gel transition upon injection [5,6] and provide localized drug delivery [7,8]. Thanks to its high swelling ability and gelation properties, hydroxypropyl methylcellulose (HPMC) has revealed as one of the most suitable materials for drug delivery purpose [9,10]. It is a cellulose derivative obtained from substitution of hydroxyl groups with alkyl or hydroxyalkyl groups to increase its solubility in water. It is considered as a low cost and ageless renewable green material with high biocompatibility, biodegradability and non-toxic properties [11,12]. Its use in commercial pharmaceutical products is already implemented in coating of oral drug delivery systems, and only recently its study has spread in hydrogel field for drug release purposes [13–15]. However, the high hydrophilicity of hydrogels limits the release of soluble therapeutics such as proteins, antibodies and soluble compounds, while preventing an effective loading of hydrophobic and low steric hindrance drugs, which are commonly used to treat many diseases [16–19]. For this class of molecules, one of the most widely explored DDS is represented by polymer nanoparticles (NPs) [20–23]. These nanosystems comprise a hydrophobic microenvironment suitable for drug loading and a stabilizing hydrophilic external corona that can provide high colloidal stability, protecting drugs from degradability, low solubility, fast clearance and immune response [24–26]. The recent

* Corresponding author.
E-mail address: filippo.rossi@polimi.it (F. Rossi).

https://doi.org/10.1016/j.ijbiomac.2024.137659
Received 11 September 2024; Received in revised form 28 October 2024; Accepted 12 November 2024
Available online 17 November 2024

advent of stimuli-responsive NPs greatly expanded their applications, paving the way to the release of active principles only when specific external conditions occur [27,28]. In particular, pH-responsive nanoparticles could be highly effective in specific sites of the body where acidic or alkaline environments are present [29]. Despite these appealing advantages, a major limit of NPs is their poor accumulation in the target area, which can induce side effects in healthy highly vascularized tissues and organs [30,31]. In this context, nanocomposite systems represents a promising strategy to tackle the limitations associated to each single system [32,33].

During the last years, nanocomposite HPMC-hydrogels based on nanoparticles loaded into HPMC matrix have gained high attraction in biomedical application area [34–37]. Several works from Appel and coworkers are related to the use of organic NPs for the development of nanocomposite HPMC-hydrogels, also called as polymer-nanoparticle hydrogels [38,39]. Their studies focused on the improvement of mechanical properties of cellulose-based hydrogels by the use of polylactic acid-polyethylene glycol (PLA-PEG) NPs [40] [41]. Despite the potential ability of these systems in achieving a controlled drug release both from organic NPs and hydrogel, few formulations were tested to study the co-delivery mechanism [42,43]. In particular, release rate of low molecular weight molecule (4 kDa) was measured from NPs and polymer, and the difference in kinetic release was considered useful for therapeutic timing to treat different stages of disease and enhance the final therapeutic effect [43]. In an other work [42], sustained codelivery of low and high molecular weight therapeutic molecules was achieved by linking the low molecular weight molecule (adjuvant (TLR7/8a)) to NPs in order to increase the molecular size and decrease the release rate. The codelivery of high and low steric hindrance molecules is becoming an important factor and its efficacy is confirmed by several phase 3 clinical trials done in the last 5 years, which prove an improved progression-free survival in patients treated with antibody plus chemotherapy than only chemotherapy [44–52]. In this work we showcase a new pH-responsive nanocomposite system with the aim of providing localized drug release of low and high steric hindrance drugs from NPs and polymer network. Indeed, we improved the available systems introducing uniform and reproducible NPs, synthetized by controlled polymerization technique and characterized by pH-responsive property. This characteristic add a further degree of control in drug release, exploiting natural gradients of pH observed in living organisms. In particular, the synthesis of homogeneous pH-responsive ((polyhydroxyethyl methacrylate-*graft*-lactic acid$_{12}$)-*co*-polymethacrylic acid)-b-polydi(ethylene glycol) methyl ether methacrylate (((PHEMA-*graft*-LA$_{12}$)-*co*-PMAA)-b-PDEGMA).

NPs was achieved by a ring opening polymerization (ROP) of D,L-Lactide followed by two consecutive reversible addition-fragmentation chain transfer (RAFT) polymerization steps forming the first and second blocks. The reproducibility and control over polymerization were assessed by proton nuclear magnetic resonance spectroscopy (^{1}H NMR) analysis and size-exclusion chromatography. After nanoparticles formation by polymer nanoprecipitation, NPs properties and pH-responsivity were analysed by DLS, TEM and UV analyses. Mimetic drugs and 5-fluorouracil (5-Fu) release tests were evaluated at different pH values, and in-vitro biocompatibility and cytotoxicity experiments were performed. Following the HPMC-C$_{12}$ synthesis reported by Appel and coworkers [40] and taking their HPMC-C$_{12}$ hydrogel as model, we created 5 % or 10 % *w*/w HMPC-C$_{12}$ polymer-nanoparticle systems characterized by pH-responsivity and well distributed uniform NPs. Rheological properties were evaluated and release kinetics of a mimetic protein was measured over time to simulate the release of high steric hindrance molecules from the polymer network. Hence, the present system exploit the possibility of delivering molecules with different hydrophilicity and molecular weights in localized tissue to respond to the future demands of DDS which involve the use of different drugs and therapeutic molecules at the same time, such as small molecules drugs and monoclonal antibodies, recently studied in clinical trials for particular therapeutic treatments [53–55].

2. Experimental section

2.1. Materials

D,L-Lactide (99 % purity, Merck, Darmstadt, Germany); stannous octoate (Sn(Oct)$_2$, 92.5–100 % purity, Merck); toluene (Merck); methacrylic acid (MAA, 99 % purity, Merck); 2,2′-azobis(2-methylpropionitrile) (AIBN, 98 % purity, Merck); acetone (Merck); dimethyl sulfoxide-d_6 (DMSO-d_6, Fluorochem, Hadfield, UK); 2-hydroxyethyl methacrylate (HEMA, ≥99 % purity, Merck); 4-cyano-4-[(dodecylsulfanylthiocarbonyl)sulfany]pentanoic acid (CTA, 97 % purity, Merck); Dulbecco's phosphate buffered saline (PBS, Merck); acetonitrile (ACN, Merck); tetrahydrofuran (THF; Merck); di(ethylene glycol) methyl ether methacrylate (EG$_2$MA, 95 % purity, Merck); 1-dodecylisocyanate (99 % purity, Merck); triethylamine (Merck); *N*-methyl pyrrolidone (99 % purity, Merck); hydroxypropylmethyl cellulose (HPMC, Merck); 5-fluorouracil (5-FU, ≥99 % purity, Merck); fluorescein isothiocyanate isomer I (FITC, ≥90 % purity, Merck); fluorescein isothiocyanate-dextran (FITC-DEX, Merck); phosphoric acid (H_3PO_4, Merck); hydrochloric acid (HCl, Merck); sodium chloride (NaCl, Merck) were of analytical grade purity and used as received unless otherwise noted.

2.2. Synthesis of HEMA-LA$_{12}$ macromonomer

A macromonomer based on PLA was synthesized via ring opening polymerization initiated by HEMA. In particular, Sn(Oct)$_2$ (0.014 g, 0.035 mmol) and D,L-Lactide (6 g, 41.63 mmol) were dissolved in 60 mL of toluene under stirring. HEMA (0.892 g, 6.94 mmol) was added to the reaction and the mixture was heated to 130 °C under constant magnetic stirring for 4 h. At the end of reaction toluene was removed under vacuum and no further purification was needed due to the high monomer conversion. The theoretical degree of polymerization (DP) was 12. Monomer conversion calculated by NMR analysis and GPC analysis was used to estimate the final molecular weight. The details on the characterization techniques are reported in Section 2.8.

2.3. Synthesis of (PHEMA-graft-PLA)-co-PMAA

Statistical copolymers of the HEMA-LA$_{12}$ macromonomer and methacrylic acid were synthesized via RAFT polymerization in hermetically sealed pyrex vials (10 mL). The previously synthetized macromonomer (1.599 g, 1.656 mmol), MAA (0.145 g, 1.656 mmol), CTA (0.028 g, 0.069 mmol) and AIBN (0.00378 g, 0.023 mmol) were dissolved in acetonitrile (5 mL) under constant stirring. The solution was purged by bubbling nitrogen for 30 min and heated to 70 °C. The reaction continued under constant magnetic stirring for 24 h. Samples were taken at 1, 2, 4 and 24 h from the reaction to evaluate the monomer conversion by NMR analysis. GPC analysis was conducted at the end of polymerization to determine the final molecular weight distribution.

2.4. Synthesis of ((PHEMA-graft-LA$_{12}$)-co-PMAA)-b-PDEGMA

The statistical (PHEMA-graft-LA$_{12}$)-co-PMAA macromolecular chain transfer agent was chain-extended with EG$_2$MA to obtain block copolymers. The RAFT polymerization was performed in hermetically sealed pyrex vials (10 mL). The obtained macro-CTA (PHEMA-graft-LA$_{12}$)-co-PMAA (0.028 g, 0.069 mmol), EG$_2$MA (0.632 g, 3.45 mmol) and AIBN (0.00378 g, 0.023 mg) were dissolved in 5 mL of acetonitrile under constant magnetic stirring. The solution was purged by bubbling nitrogen for 30 min and heated to 70 °C. The reaction continued under constant magnetic stirring for 24 h. For each reaction, samples were taken at different time points in order to track monomer conversion during time by NMR analysis. GPC analysis was performed at the end of the reaction to calculate the final molecular weight distribution of the polymer.

2.5. HPMC-C_{12} functionalization

HPMC functionalization with alkyl chains of twelve carbons was performed according to the procedure disclosed by Appel and coworkers [39,40].

HPMC (1 g, 0.01 mmol) was dissolved in *N*-methylpyrrolidone (45 mL) under constant stirring for 1 h at 80 °C. After HPMC was completely dissolved, the mixture was cooled to room temperature. A mixture of 1-dodecyl isothiocyanate (0.120 mL), triethylamine (2 drops) and *N*-methylpyrrolidone (5 mL) was added to the reaction. The reaction proceeded at room temperature under constant stirring for 16 h. The product was precipitated in acetone and filtrated. Finally, the functionalized HPMC was dissolved in water and dialyzed against distilled water for 48 h before lyophilization.

2.6. Nanoparticles production and characterization

NPs were produced via nanoprecipitation from the block copolymers ((PHEMA-graft-LA_{12})-co-PMAA)-b-PDEGMA. In particular, 50 mg of polymer were dissolved in 1 mL of acetonitrile, and the solution was added with a 20–200 μL pipette dropwise to distilled water (10 mL) maintained under magnetic stirring at 600 rpm in a 25 mL glass vial. After nanoprecipitation, the nanoparticle suspension was kept under stirring for at least 30 min.

2.7. Drug loading and release from nanoparticles

NPs were loaded with molecules characterized by different hydrophilicity to study their effect on drug release [56]. In particular, rhodamineB/FITC/pyrene/5-FU-loaded NPs were produced by using the same procedure as reported in Section 2.6, with the addition of rhodamine B, FITC, pyrene or 5-FU to acetonitrile at 2 mg/mL concentration. 3 mL of NP solution were dialyzed by using 3.5 kDa cellulose membranes against 40 mL PBS for 30 min under magnetic stirring. After that the PBS was totally removed to calculate the encapsulation efficacy and the drug loading, as follows (Eqs. (1) and (2)):

$$\%\mathrm{Eff} = \left(1 - \frac{C_v}{C_0}\right) \bullet 100 \quad (1)$$

$$\%\mathrm{DL} = \left(\frac{m_{ed}}{m_{ed} + m_p}\right) \bullet 100 \quad (2)$$

where %Eff is the encapsulation efficiency, C_0 is the drug concentration at the initial time and C_v is the concentration of drug recovered in the external medium. In the Eq. (2), %DL refers to the drug loading, m_{ed} to the mass of encapsulated drug and m_p to the mass of polymer. After the washing step, 40 mL of fresh PBS or 0.01 M phosphate buffer at pH = 2 were replaced, and the systems kept at 37 °C to study the drug release at different pHs. For each release system, 2 mL of external medium were withdrawn at different time intervals and replaced with fresh solution to maintain the external volume constant. The samples containing the 5-FU were analysed by high-performance liquid chromatography (HPLC) with UV detection. Analyses were conducted using a Roc C18 5 μm 250 × 4.6 mm column and a mobile phase composed by 1.2 % *v*/v acetic acid, 58.8 % v/v distilled water and 40 % v/v acetonitrile with a flow rate of 1 mL/min and 10 min run time. The samples containing rhodamine B, pyrene or FITC were analysed by UV–Vis analyses performed on a Jasco V-630 spectrophotometer. The absorbance was measured at 430 nm and 490 nm for FITC dissolved in acidic (pH = 2) or neutral (pH = 7) phosphate buffer, respectively. The absorbance was measured at 335 nm and 540 nm for pyrene and rhodamine B, respectively.

2.8. Characterization of polymers and NPs

Polymer composition and monomer conversion were characterized by ^{1}H NMR analyses, performed by dissolving 20 mg sample in 0.6 mL of DMSO-d_6. The analysis was performed on a 400 MHz apparatus (Bruker), with 128 scans per sample. Molecular weight distribution of polymers was measured by GPC size exclusion chromatography (SEC) performed using THF as eluent with a flow rate of 1 mL/min at a temperature of 35 °C. Samples of polymer were dried under vacuum and dissolved in THF to obtain a final concentration of 4 mg/mL and filtrated with PTFE 0.45 μm filter before the analysis.

The instrument (Jasco 2000 series) was equipped with a differential refractive index (RI) detector and three PL gel columns (Polymer laboratories Ltd., UK; two columns had pore sizes of the MXC type and one was an oligopore; 300 mm length and 7.5 mm ID) and a precolumn. A calibration with polystyrene (PS) standards from 580 Da to 3,250,000 Da (Polymer Laboratories) was performed. The particle size distribution and pH-responsivity of NPs were studied by dynamic light scattering (DLS) using a Malvern Zetasizer Nano ZS at a scattering angle of 173° (backscatter). Measurements of the hydrodynamic diameters were performed at different pH water-solutions from 1 to 14. Three measurements were conducted with an equilibration time of 120 s before data recording. The size and morphology of produced NPs were also confirmed by TEM (using an EFTEM Leo 912AB, at 80 kV, by Karl Zeiss, Jena, Germany). Samples were prepared by placing a 5 mL drop of NP dispersion on a Formvar/carbon-coated copper grid and dried overnight. Digital images were acquired by using a charge- coupled device (CCD; Esi Vision Proscan camera). Optical transmittance measurements of NPs in water solutions at different pH conditions were performed by Jasco V-630 UV–vis spectrophotometer. Transmittance of nanoparticle suspensions were measured at 500 nm. Critical micellar concentration (CMC) was measured by Jasco FP8500 spectrofluorometer. In particular, a specific amount of pyrene dissolved into acetone was inserted to different glass vials and acetone was let to evaporated. Different concentrations of aqueous polymer solutions from 5000 mg/L to 0.001 mg/L were added to the vials reaching a final pyrene concentration of 6×10^{-7} M in each vial. Vials were stored in the dark for 24 h before the spectrofluorimetric analysis. Excitation was carried out at 335 nm and emission spectra was recorded between 350 and 450 nm. Band widths were set at 5 and 2 nm for excitation and emission, respectively. Intensity ratio (I_3/I_1) of the third band (384 nm, I_3) to the first band (373 nm, I_1) of the pyrene emission spectra was used to characterize the polarity of environment [57].

2.9. Cell metabolic activity

HeLa cells, derived from human epithelial cervical carcinoma, were cultured in Dulbecco's modified Eagle's medium-high glucose (DMEM, high glucose) supplemented with 10 % fetal bovine serum (FBS), 1 % penicillin-streptomycin, and 1 % L-glutamine. Cells were maintained in a humidified incubator at 37 °C with 5 % CO_2. The metabolic activity of the cells was assessed using the MTT assay (Merck, Germany) after NP administration. HeLa cells were seeded at a density of 5×10^3 cells per well in a 96-well plate and cultured in a humidified atmosphere (5 % CO_2) at 37 °C in complete medium for 24 h. For the biocompatibility test cells were then administered with different concentrations of NPs for 24 h. After incubation with the NPs, the culture medium was replenished with 100 μL of MTT solution (0.5 mg/mL) in complete medium and incubated for 3 h at 37 °C. The solution was carefully removed, and 100 μL of DMSO were added to each well to solubilize the resulting formazan crystals. Finally, the absorbance of the resulting solutions was measured spectrophotometrically (570 nm). Absorbance values were normalized to those of untreated cells, which represent the negative control group. For the cytotoxicity test, HeLa cells were then divided into four groups: one treated with a negative control, one treated with 5-FU at a concentration of 2.6 μg/mL, one treated with NPs at a concentration of 0.1 mg/mL, and one treated with the drug encapsulated in the NPs [58]. Pristine NPs, free 5-Fu and untreated cells were utilized as control groups for the designed experimental setup. For each experimental set,

three multiwell plate were used to assess cell viability at 24, 48, and 72 h. For each time, the MTT solution was carefully removed, and 100 μL of DMSO was added to each well to solubilize the resulting formazan crystal. The absorbance was analysed spectrophotometrically at 570 nm. The percentage values of triplicate, expressed as mean ± standard deviation, are reported with respect to untreated cells, which represent the negative control group.

2.10. HPMC-C_{12}-based systems production

HPMC-C_{12} 5 wt% and HPMC-C_{12} 10 wt% formulations were obtained by mixing the lyophilized HPMC-C_{12} with PBS in a 25 mL glass vial under shaking (Heidolph Instruments, Schwabach, Germany) at 1000 rpm for 48 h. NP-loaded materials were produced in the same way by using NP suspensions at different concentrations instead of PBS in order to obtain a HPMC-C_{12}:NPs (wt%) of 1:2 and 1:4 for the HPMC-C_{12} 5 wt% and 1:1 for the HPMC-C_{12} 10 wt%.

2.11. FITC-DEX loading and release from composite systems

Preliminary tests of FITC-DEX loading and release were performed using HPMC-C_{12} 5 wt% and HPMC-C_{12} 10 wt% formulations without NPs (HPMC-C_{12}:NPs wt% of 1:0). The same procedure described in the previous section was adopted to form the final polymer network, but a 1 mg/mL FITC-DEX solution in PBS was used. First, 20 mL of PBS were added above the system and removed after 30 min in order to calculate the encapsulation efficiency of polymer networks, as reported above. Then 20 mL of fresh PBS were added, and 1 mL of supernatant was withdrawn at different time intervals and replaced with fresh PBS to study the release profile. Concentration of FITC-DEX in each sample was analysed by measuring the absorbance at 495 nm (BioTek Synergy™ H1 multi-mode microplate reader) against a calibration curve.

2.12. Characterization of composite systems

Functionalization of HPMC into HPMC-C_{12} was evaluated by ATR-FTIR spectroscopy using a Varian 640-IR spectrometer equipped with a single bounce ZnSe ATR accessory on lyophilized HPMC-C_{12}. Oscillatory rheological measurements were performed to study the rheological properties of systems. The equipment used was an Anton Paar MCR502 with PP25/P2 plates and a Peltier H-PTD 200 temperature-controlled plate and hood. Shear strain amplitude sweeps were carried out at shear strain amplitudes ranging from 0.1 to 1000 % and at the constant angular frequency of 10 rad/s.

Frequency sweep tests were carried out at an angular frequency ranging from 1 to 300 rad/s and at the constant shear strain of 0.01 %; temperature was 25 °C and 37 °C. Polymer network surface morphology was evaluated using Extended pressure SEM (Zeiss EVO 50 EP). Systems were freeze-dried by VirTis BenchTop Pro with Omnitronics (SP Scientific) at −20 °C for 24 h and coated with gold (Edwards S150B Sputter coater).

2.13. Statistical analysis

The experimental data were analysed using Analysis of Variance (ANOVA). Statistical significance was set to p value <0.05. Results are presented as mean value ± standard deviation.

3. Results and discussion

3.1. ((PHEMA-graft-LA_{12})-co-PMAA)-b-PDEGMA synthesis and characterization

((PHEMA-*graft*-LA_{12})-co-PMAA)-b-PDEGMA copolymer was synthesized via a combination of ROP and RAFT polymerization, as schematically shown in Fig. 1. In particular, PLA-based macromonomer was obtained via ROP, using HEMA as initiator in the presence of $Sn(Oct)_2$ as catalyst. In order to precisely control the chain length, the molar ratio of

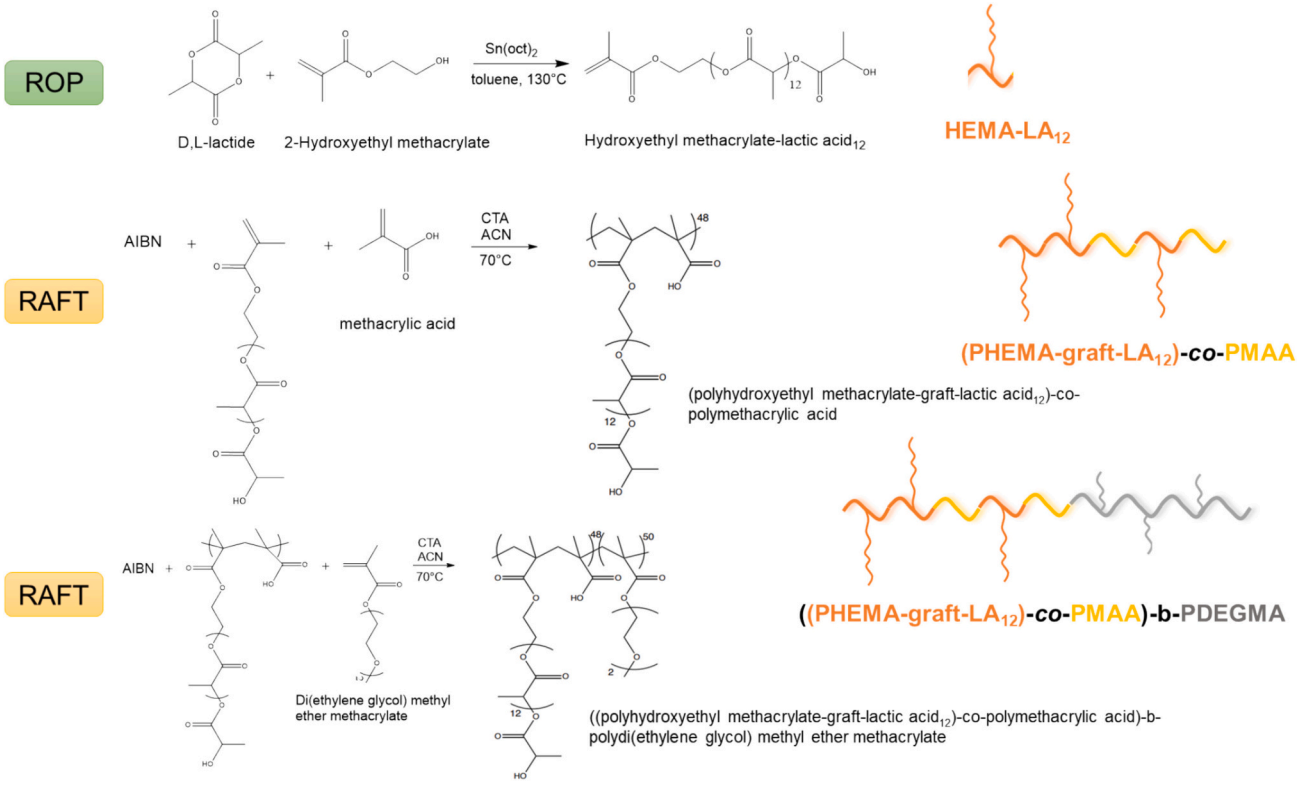

Fig. 1. Scheme of polymerization reactions performed sequentially for the synthesis of ((PHEMA-*graft*-LA_{12})-*co*-PMAA)-b-PDEGMA copolymer.

D,L-Lactide:HEMA was adjusted to 6:1. The monomer conversion was confirmed by the resonance peak of PLA obtained at 5.2 ppm from the ^{1}H NMR analysis (Fig. S1). The number average molecular weight (M_n) of PLA was calculated from ^{1}H NMR spectrum according to Eq. 3.

$$M_{n\,HEMA-LA_{12}} = MW_{HEMA} + MW_{LA} \bullet \left(\frac{\int f_{proton\ signal}}{\int a_{proton\ signal}} + 1 \right) \quad (3)$$

where MW_{HEMA} and MW_{LA} are, respectively, the molecular weight of HEMA and D,L-Lactic acid, whereas $\int f_{proton\ signal}$ and $\int a_{proton\ signal}$ represent the area under the curve of peaks *f* and *a* respectively (Fig. S1). The resulting Mn was 982 Da. Copolymerization of HEMA-LA_{12} and MAA was performed by RAFT polymerization using 4-Cyano-4-[(dodecylsulfanylthiocarbonyl) sulfanyl] pentanoic acid as chain transfer agent and a HEMA-LA_{12}:MAA molar ratio of 1:1. The choice of using MAA is to provide pH responsivity to the final polymer. The pH responsivity derived from protonation and deprotonation equilibrium, which occurs on carboxyl group at different pH conditions. The ^{1}H NMR spectrum of the reaction product is shown in Fig. S2. The RAFT polymerization was performed multiple times to assess the conversion reproducibility over time. The conversion of each monomer was calculated at different time intervals by using the following formulas:

$$\text{Conversion}\ (\%)_{HEMA-LA_{12}} = \left(1 - \frac{\int a_t}{\int f}\right) \bullet 100 \quad (4)$$

$$\text{Conversion}\ (\%)_{MAA} = \left(1 - \frac{\int b_t}{\int f}\right) \bullet 100 \quad (5)$$

where $\int a_t$ represents the area under curve of peak a at time t, and $\int f$ represents the area under curve of peak f (Fig. S2), which was the reference integral, so it was maintained always at the same value.

Fig. 2 shows the conversion of HEMA-LA_{12} and MAA into polymer of six reactions performed at the same reaction conditions. By looking at the linear semilogarithmic plot in Fig. 2b, it is possible to conclude that a constant concentration of radicals is present in the reaction environment, due to the absence of termination reactions typical of RAFT polymerization. This testifies the good control over the polymerization during the whole time interval, which is pivotal to properly govern the polymer properties. For the last step of the copolymer synthesis, RAFT polymerization of DEGMA monomer was performed (Fig. S3). In this case the previously synthetized (PHEMA-graft-LA_{12})-co-PMAA was used as macro-CTA, so only the monomer and AIBN were added.

In particular, the addition of AIBN was performed in order to achieve a macro-CTA:AIBN molar ratio of 3:1. The reaction was repeated systematically to ensure the kinetic reproducibility. Fig. 2 shows the conversion during time for the RAFT polymerizations, where the small standard deviation indicates a good reproducibility of results. High monomer conversions (> 95 %) were obtained after 24 h. As discussed for the macro-CTA, the semilogarithmic plot of monomer conversion in Fig. 2d shows a liner trend, demonstrating the control over the polymerization. Polymers synthesized at each step were analysed by ^{1}H NMR and GPC (Fig. S1, S2, S3 and S4) and the relative conversions, DP and average molecular weights are shown in Table 1.

3.2. NP synthesis and characterization

Nanoprecipitation of the final ((PHEMA-graft-LA_{12})-co-PMAA)-b-PDEGMA was performed in water to form NPs. Fig. 3a shows a TEM

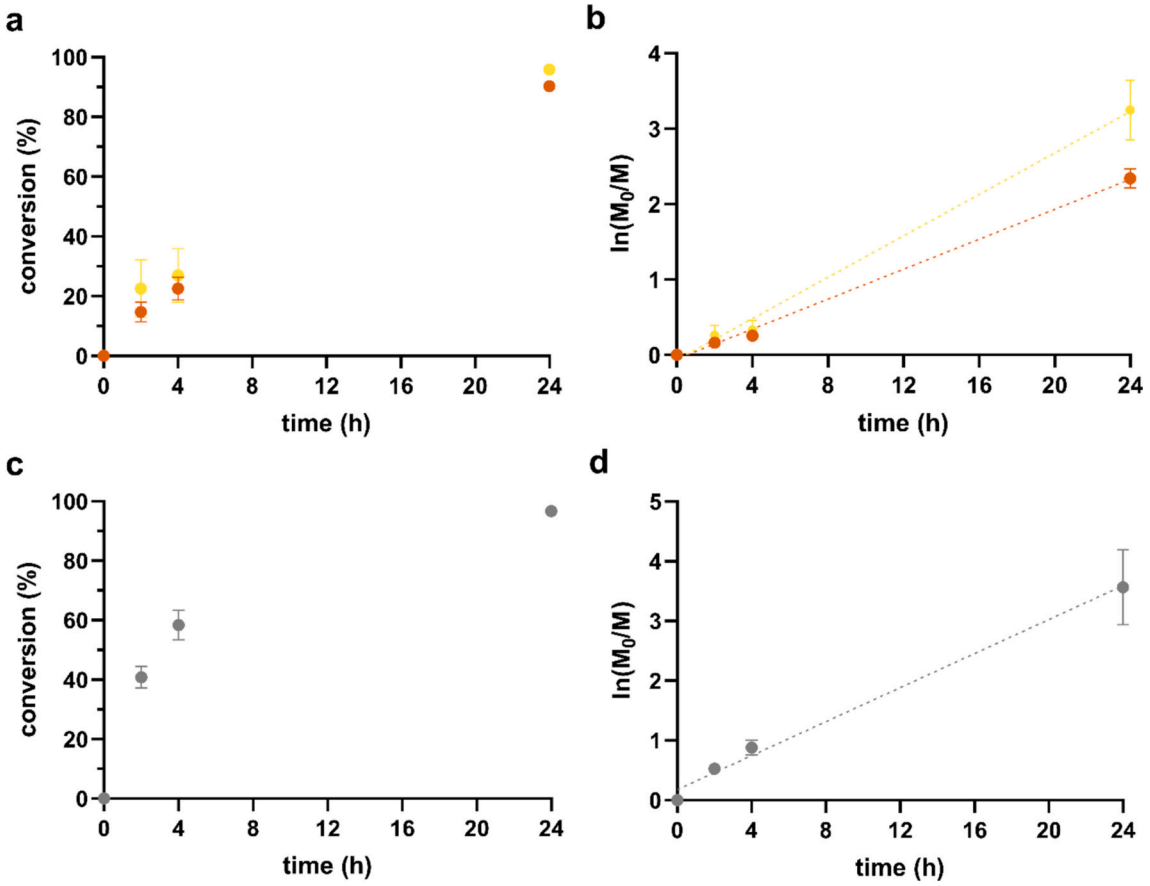

Fig. 2. (a, b) Conversion percentages and semilogarithmic plot of monomer conversions over time for the RAFT polymerization of HEMA-LA_{12} (orange) and MAA (yellow). (c, d) Conversion percentage and semilogarithmic plot of DEGMA (grey) conversion in the RAFT polymerization mediated by the (PHEMA-*graft*-LA_{12})-*co*-PMAA macromolecular chain transfer agent.

Table 1
Conversion and average molecular weights of polymers calculated as mean ± standard deviation at the end of each polymerization step by ^{1}H-NMR and GPC analyses.

Polymerization step	Conversion (%)	DP	^{1}H NMR	GPC		
			M_n (Da)	M_n (Da)	M_w (Da)	PDI (−)
HEMA-LA_{12}	90.2 ± 0.9	10.8 ± 0.12	1000 ± 10	650 ± 100	1400 ± 150	2.20 ± 0.15
(PHEMA-graft-LA_{12})-co-PMAA	90.3 ± 1.25 (PLA) 95.8 ± 1.49 (MAA)	21.7 ± 0.29 (PLA) 22.9 ± 0.35 (MAA)	25,000 ± 300	15,500 ± 500	20,000 ± 300	1.20 ± 0.02
((PHEMA-graft-LA_{12})-co-PMAA)-b-PDEGMA	96.7 ± 2.18	48.4 ± 1.09	30,000 ± 300	20,000 ± 700	25,000 ± 700	1.25 ± 0.03

^{1}H-NMR and GPC analyses provided average molecular weights in good agreement. The lower values obtained from GPC chromatography could be related to the different type of polymer used for the calibration of the instrument, in this case polystyrene. Low values of polydispersity index guaranteed the control over polymerization in case of polymers synthesized by RAFT polymerization.

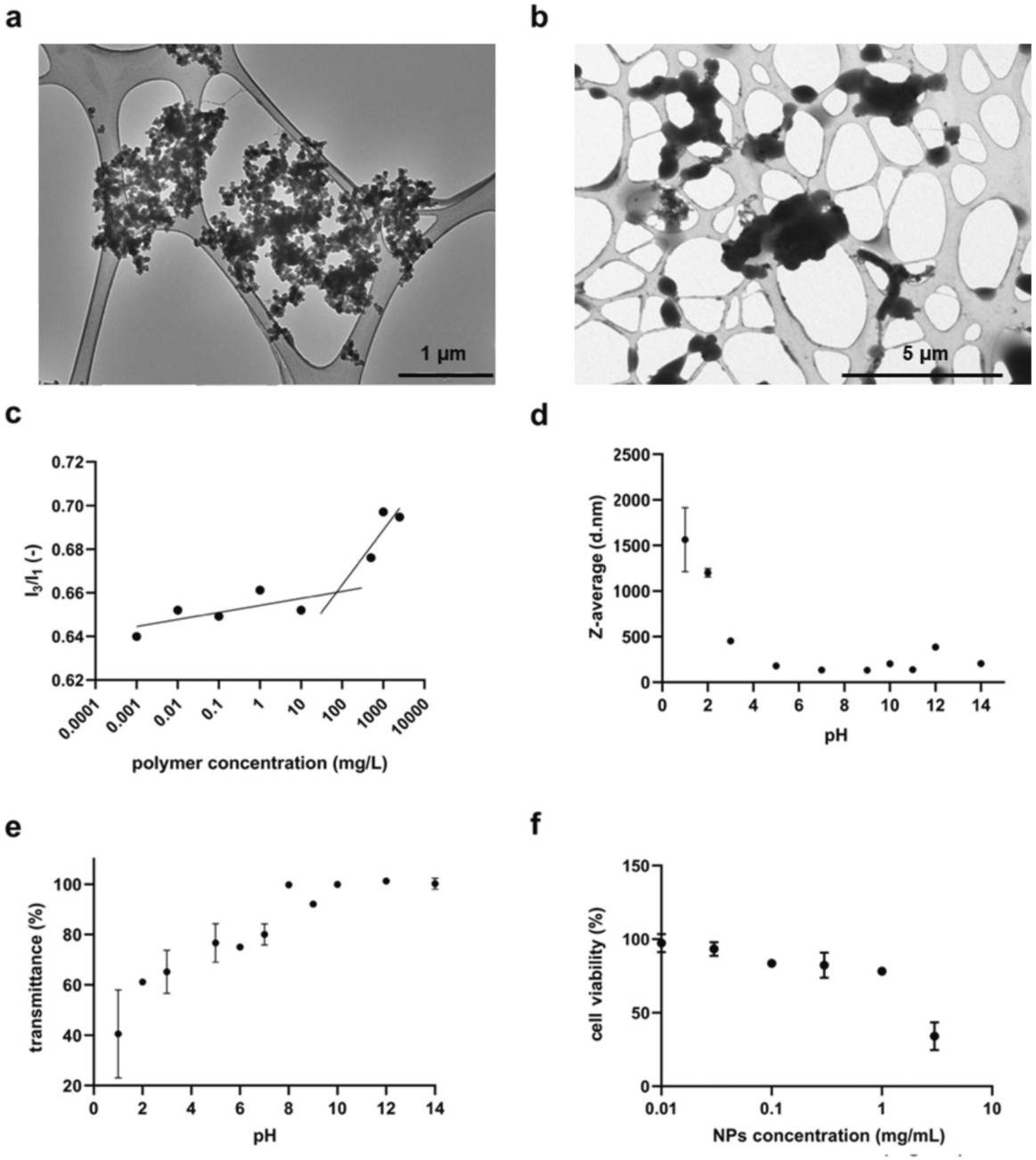

Fig. 3. TEM image of (a) nanoparticle solution on grid after incubation at neutral pH; (b) NPs on grid after incubation in acidic pH solution. Graph of (c) I_3/I_1 vs. polymer concentration showing the CMC of the final copolymer; (d) *Z*-average of NPs at different pH solutions (e) UV–vis results of nanoparticle solution transmittance at different pH; (f) percentage of cellular viability vs nanoparticle concentrations from in vitro biocompatibility test.

image of a single NP at neutral pH with a diameter around 150 nm. TEM images of NP solution at neutral pH (Fig. 3b) and pH = 2 (Fig. 3c) show a different behaviour of NPs. In particular, NPs can be individually identified in neutral pH (additional images on Fig. S5a and S5b of Supporting information) due to their high stability, whereas they are presented in agglomerated forms in case of acidic pH.

The resulting phenomenon is a consequence of methacrylic acid protonation which occurs in acidic pH and leads to changes of intra and inter polymer interactions. In particular, the lower solubility of MAA in its protonated form is responsible for the NP destabilization and formation of large aggregates [59], as revealed by both TEM and DLS. The CMC of the amphiphilic polymer was measured to study the concentration at which the formation of hydrophobic regions associated to the copolymer self-assembly into NPs occurs (Fig. 3c). Pyrene was used as a tracer due to its hydrophobicity and stability in nonpolar solvents [60]. Low values of I_3/I_1 between 0.64 and 0.66 were maintained for low polymer concentrations, indicating that the pyrene was dispersed in the aqueous phase and no micelles were present. By increasing the polymer concentration, an increase of I_3/I_1 value up to around 0.7 was evident, testifying the formation of hydrophobic microenvironments where pyrene was incorporated and stabilized. From this analysis, the CMC was taken as the concentration leading to a change in the slope of the ratio I_3/I_1. A CMC of 70.8 mg/L was obtained, in agreement with values reported in the literature for similar copolymers (10^{-7}–10^{-5} M) [61,62]. Indeed, this result confirmed the micellar formation starting from ((PHEMA-graft-LA_{12})-co-PMAA)-b-PDEGMA copolymer and its potential use for drug delivery purpose. In agreement with TEM results, DLS analysis of nanoparticles at neutral pH revealed a *Z*-average size of 154 nm and a polydispersity of 0.14. The same analysis was performed with a gradient of temperature over a temperature range between 20 and 60 °C to demonstrate the stability of NPs at physiological temperature and up to higher temperature conditions (Fig. S6). Z-average measurements remain stable between 150 and 160 nm with a polydispersity of 0.15. DLS analysis was also conducted at different pH values in order to study the effect of pH on NPs behaviour. Fig. 3d represents the results of Z-average at different pH values. An increase in NP size was observed for pH values ≤3, where the average hydrodynamic diameter reached values up to 1600 nm. In fact, as reported in literature, the increase of hydrophobicity after the protonation could lead to structural changes of NPs and subsequent formation of aggregates [63,64].

The partial accordance between DLS and TEM analyses is due to the different technology used: wet for DLS and dry for TEM. The pH-responsivity was also verified by UV–vis analysis, in which the transmittance measured at 500 nm revealed different values depending on the pH of the suspension. Fig. 3e shows a decrease of transmittance by decreasing the pH from 14 to 1. Indeed, the intensity of the scattered light is directly proportional to the NP diameter at the sixth power. Hence, this decreased transmittance when moving to acidic pH further confirms the gradual protonation of carboxyl groups followed by the formation of large scatterers, responsible for an increase in the suspension turbidity. Biocompatibility of NPs was assessed performing MTT tests on HeLa cells supplemented with NPs at different concentrations and results showed good cellular viability up to 1 mg/mL (Fig. 3f).

3.3. Drug release

The effect of pH-responsive behaviour of NPs on drug release was studied firstly by using rhodamine B, FITC and pyrene as drug mimetics, respectively, hydrophilic highly soluble molecules, relatively hydrophilic poorly soluble ones and hydrophobic insoluble ones. Considering the differences in chemical and physical properties between molecules, it was assumed that after the drug loading, rhodamine B was mainly located in the hydrophilic shell, whereas FITC and pyrene were entrapped in the core of NPs. The release of each molecule from NPs was performed at 37 °C in acidic (pH = 2) and neutral (pH = 7) buffer as described in Section 2.7. An extreme acidic condition (pH = 2) was used for release studies to assess the effectiveness of drug release at pH < <pKa of MAA, where NPs have already exhibited pH responsivity. However, this extreme experimental condition does not exclude the possibility of having an enhanced drug release also for higher pH values, as can be deduced from the characterization evidence at different pHs (see Fig. 3e). Encapsulation efficiency of FITC and pyrene were respectively 93.5±8.3 % and 83.1±3.2 %, confirming the high interaction of the molecules with the core of NPs, whereas only 77.1±7.3 % of rhodamine B was loaded inside NPs. Lower value of encapsulation for rhodamine B could be explained by the hydrophilicity of the molecule which is more favoured to stay in the water environment. Considering these differences in encapsulation efficiency, the respective drug loading values were 3.0±0.5 % for rhodamine B, 3.6±0.3 % for FITC and 3.2 ±0.4 % for pyrene. Drug release from NPs was finally tracked during time, as shown in Fig. 4a.

Controlled and sustained release was evidenced for all the mimetic drug molecules. Drug release of FITC and pyrene in PBS buffer had similar trends and reached very low value of cumulated release, below 20 % of the total encapsulated molecule. The low value of release is due to the hydrophobicity and/or low solubility of the molecules and their ability to restrain from diffusion to the external environment. Opposite trend was measured in acidic buffer, where the final cumulated release for FITC and pyrene reached the values of 83 % and 90.8 %, respectively. In this case a gradual increase of release was observed up to one week for pyrene and 3 weeks for FITC, sign of a controlled and sustained release over a long period of time. A possible explanation of the increase can be attributable to hydrogen bond interactions between protonated carboxylic groups of MAA and ethylene glycol moieties [65,66], which are responsible of following agglomeration and squeezing the drug outside the NP [67]. Indeed, a decrease of *Z*-potential from -43 mV to -4 mV was observable decreasing the pH from neutral to acidic values, indicating a possible change in oxygen interactions (data not shown).

These results demonstrated the potential use of pH-responsive NPs in modulating the release of hydrophobic and slightly hydrophilic molecules, which can be exploited for a target release of the active principle. Different mechanism of release was observed in rhodamine B release curve. Indeed, higher release was measured in PBS buffer (~87 %) compared to that in acidic pH (~60 %). One reason could be associated to the open conformation of rhodamine B in acidic solution, which can form hydrogen bonds between carboxylic groups and oxygens of ethylene glycol. For both neutral and acidic pH conditions, no burst release was evidenced and sustained release was achieved up to 1 day, followed by controlled release. Logarithm of cumulated release vs. logarithm of time (Fig. 4b) was plotted following Korsmeyer-Peppas model in order to describe drug release type from a polymeric system [68]. Coefficients of linear curves are between 0.23 and 0.46, indicating a Quasi-Fickian diffusion from a non swellable matrix diffusion for all molecules. Difference between coefficients depends on geometry of particles and their polydispersity. In particular a coefficient of 0.432 ± 0.007 indicates Fickian diffusion mechanism from a polymeric sphere [69]. Release test from NPs at neutral and acidic pH were also performed using a real drug, in this case 5-Fu (Fig. 5a). Encapsulation efficiency was 64±11.3 %, and drug loading was 2.5±0.4 %. Cumulated release at neutral pH reached a value around 85 %, whereas at acidic pH it reached around 60 %. Lower release in acidic pH could be related to the lower solubility of the drug at acidic pH solution compared to the neutral one [70,71]. However, in this case burst release was observed for both pHs in the first 2 h, followed by a slower and sustained release up to 28 days. The quick release kinetic could be potentially related to the partial hydrophilic nature of 5-FU, able to easily diffuse from the surface of NPs to the external water solution. Other drugs would be tested in future to analyse their response during the first hours of release. Higher slope of linear curve section indicates a faster release in PBS compared to acid solution.

Finally, FITC-DEX release experiments from the HPMC-C_{12} system were performed to study the ability of the polymeric network in

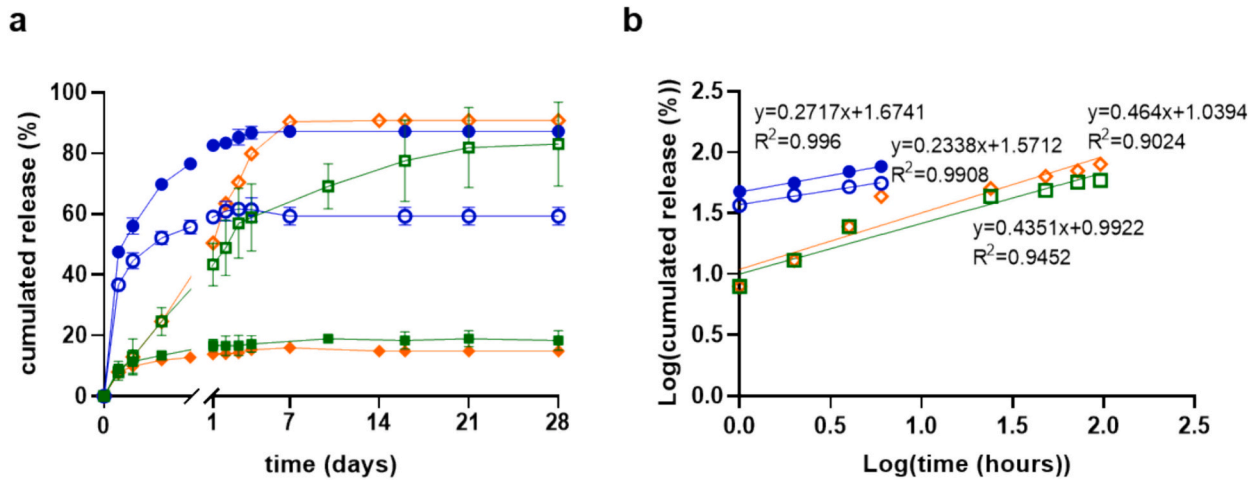

Fig. 4. (a) Cumulated release from NPs vs. time (days) (b) Log(cumulated release) vs. log(time (hours)) curve of rhodamine B (blue), pyrene (orange) and FITC (green) in PBS (full points) and pH = 2 buffer (empty points). The slope of drug release against log(time (hours)) is representative of drug transport mechanism for each sample ($p < 0.005$ between all groups).

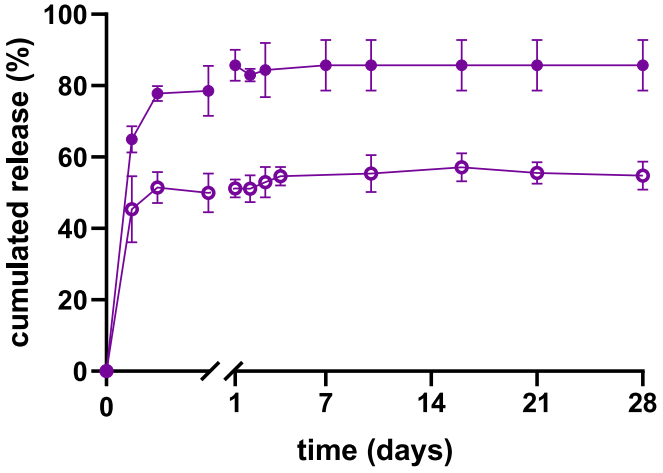

Fig. 5. Cumulated release from NPs vs. time (days) of 5-FU (purple) in PBS (full points) and pH = 2 buffer (empty points).

releasing high steric hindrance drugs or proteins characterized by similar hydrodynamic radius [72,73] and molecular weight. Two formulations at 5 wt% and 10 wt% of HPMC-C_{12} concentration were tested. FITC-DEX release experiments up to 3 weeks (Fig. 6a) showed a similar release curve and a similar release kinetic during the first hours. Both the releases reached the plateau only after two weeks, indicating a gradual and sustained release of the molecule. Higher percentage of cumulated release (70 %) was obtained from the HPMC-C_{12} 5 wt% due to the larger mesh size of the system, which is derived by the lower concentration of cellulose. High values of standard deviation were registered for the HPMC-C_{12} 5 wt%, probably due to the low stability and possible degradation of the system in water external solution. Cumulative drug release was plotted against the square root of time (Fig. 6b). The linearity of the curve indicates Fickian diffusion of FITC-DEX through the polymer matrix [59,74]. The slope of release from the HPMC-C_{12} 5 wt% is steeper compared to that of HPMC-C_{12} 10 wt%, but the linear trend was maintained for both formulations up to 7 days. This represented an important advancement in the direction of a prolonged sustained release compared to traditional formulations [19].

3.4. In vitro cell assay

In vitro cytotoxicity test was performed on HeLa cells using MTT assay, as previously discussed. Moreover, cells were treated with either a

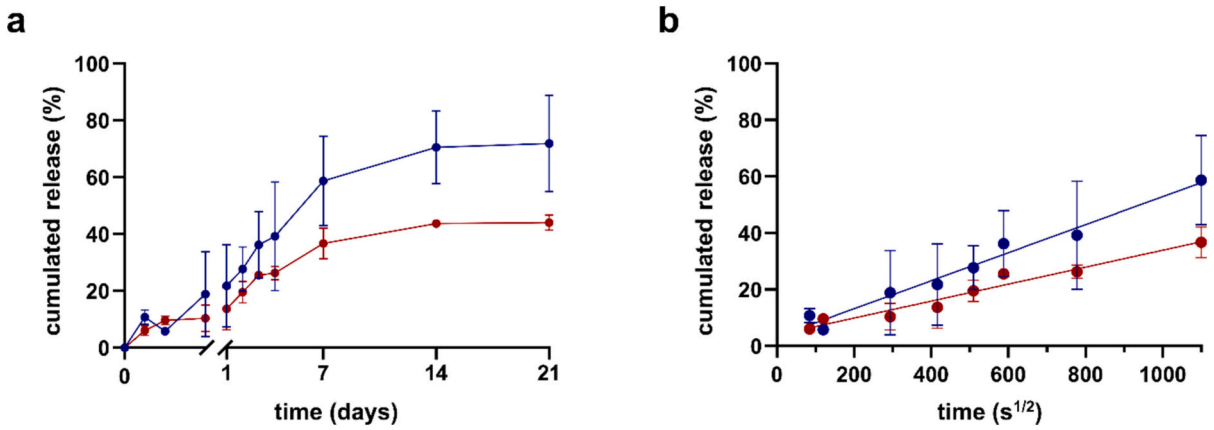

Fig. 6. (a) Cumulated release from polymer network vs. time (days) curve and (b) cumulated release vs. time ($s^{1/2}$) curve of FITC-DEX release from the HPMC-C_{12} 5 wt% (blue) and HPMC-C_{12} 10 wt% (red) in PBS. The slope of drug release against the square root of time is representative of Fickian diffusion coefficients for each sample ($p < 0.001$ between all groups).

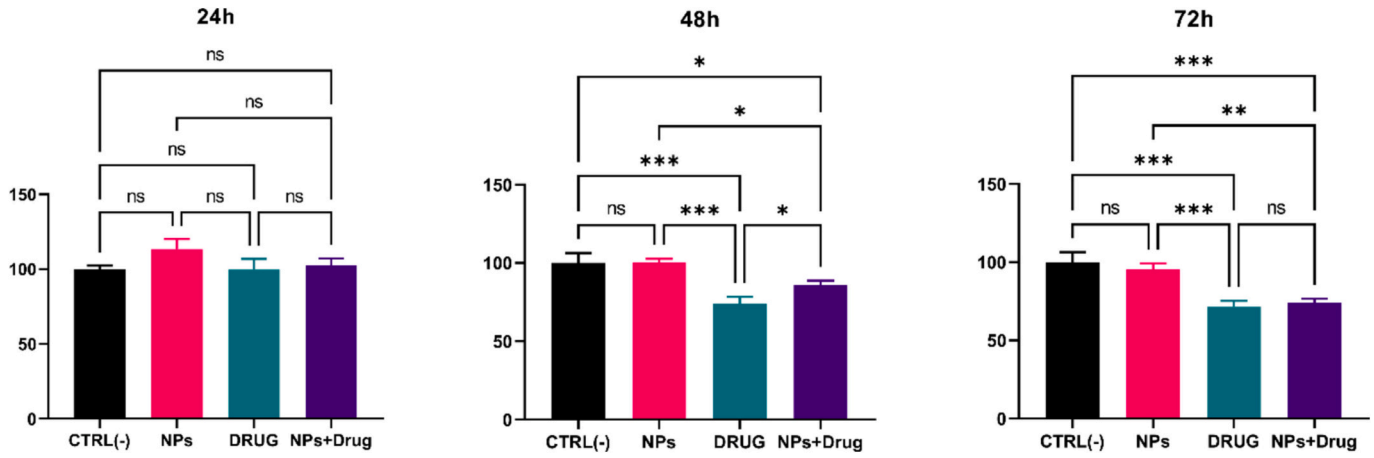

Fig. 7. MTT assay on cells untreated (black), treated with NPs (pink), 5-Fu solution (green) and 5-Fu loaded NPs (purple) at 24 h, 48 h and 72 h.

suspension of 5-Fu-loaded NPs or a solution of pure 5-Fu in PBS. Fig. 7 shows the percentage of cell viability after 24 h, 48 h and 72 h of cells untreated (black), treated with NPs (pink), 5-Fu solution (green) and 5-Fu-loaded NPs (purple). Cell viability of cells treated with NPs maintained high values over 72 h (around 100 %), whereas lower values were measured from 48 h to 72 h for samples treated with free 5-Fu and 5-Fu-loaded NPs. In particular, after an incubation of 48 h with free 5-Fu and 5-Fu-loaded NP solution the viabilities were respectively 74 % and 85 %, meaning that initially the use of the only drug had a higher effect than that with the use of NPs. After 72 h the results showed a viability of 74 % for the sample treated with 5-Fu-loaded NPs and no significant change for cells treated with the only 5-Fu. This effect demonstrated the ability of NPs in achieving a controlled release of drug over time, allowing a continuous drug release and consequent decrease of cell viability, not observable for the sample treated with the drug solution.

Therefore, in vitro outcomes evidenced the high biocompatibility of polymeric NPs and their promising use for the controlled drug release in biomedical field.

3.5. Polymer-nanoparticle composite system characterization

First, HPMC was functionalized following the procedure described by Appel and coworkers with C_{12} chains by using 1-dodecyl isothiocyanate as reagent [40]. The functionalization of a fraction of the hydroxyl groups of HPMC with hydrophobic chains allowed a better interaction between polymer network and the core of NPs, leading to a polymer network with higher mechanical properties. The correct modification was verified by IR-analysis, which showed the peaks corresponding to the functionalized polymer (Fig. S7) [40,75]. The composite system was formed following the procedure described in Section 2.10. Fig. 8a shows its schematic formation, which resulted in a homogeneous combination of HPMC-based polymer network and organic pH-responsive nanoparticles able to interact each other by associating the respective hydrophobic regions. SEM micrographs of the composite network revealed

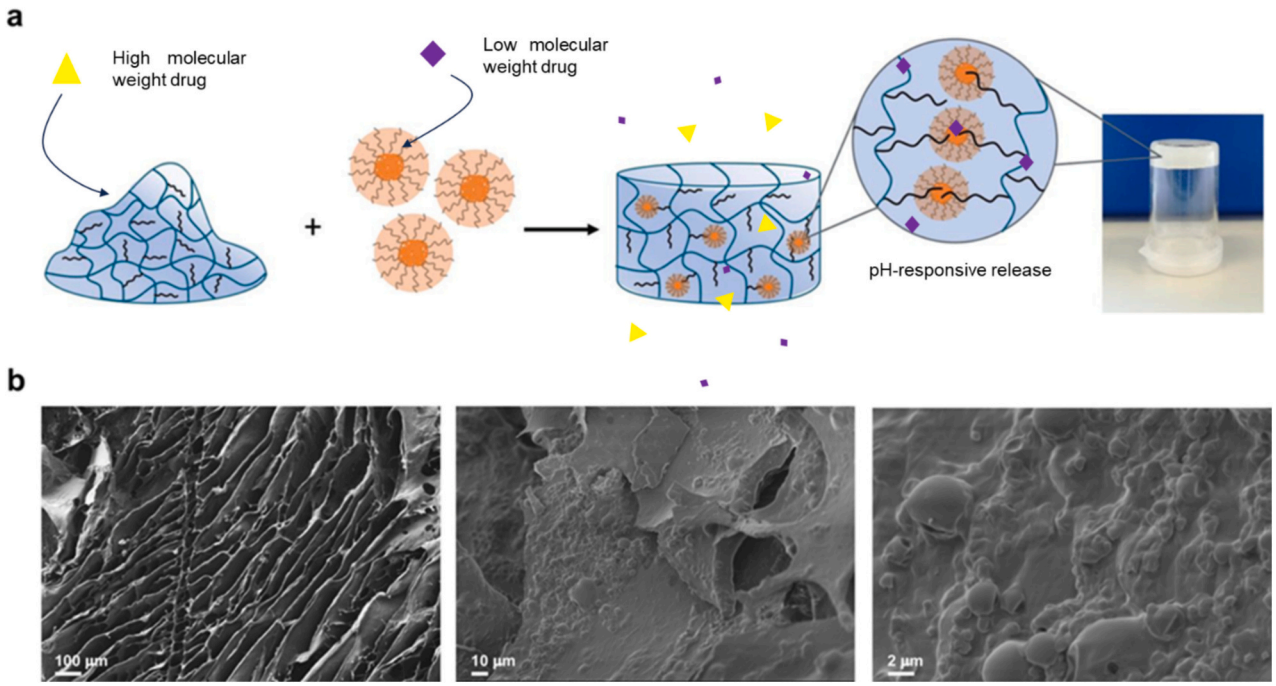

Fig. 8. (a) Scheme of polymer-NPs composite system formation, codelivery mechanism and visual picture of the resulting material. (b) SEM images of the composite network that demonstrate a homogeneous distribution of NPs within the gel structure, indicating that the network is held together by polymer-nanoparticle interactions.

a lamellar structure comprising sheets of HPMC-C_{12}. The surface of the single sheet was characterized by short filaments which protrude in perpendicular way typical of cellulose-based hydrogels (Fig. 8b) [40,76,77]. At higher magnification the presence of spherical-shape particles on the surface of sheets is well visible.

The size of these NPs resulted higher than that obtained by DLS analysis, due to the limitation of this technique to observe nano systems.

The two different formulations with HPMC-C_{12} content at 5 wt% and 10 % were also characterized for their mechanical properties. Amplitude sweep tests on HPMC-C_{12} 5 wt% and HPMC-C_{12} 10 wt% formulations were performed in a range of shear strain between 0.01 and 1000 % (Fig. 9a). For both the compositions, a broad linear viscoelastic region up to 10 % of shear strain was measured. A solid-like viscoelastic behaviour was highlighted for the HPMC-C_{12} 10 wt% system (G' > G"), whereas a liquid-like viscoelastic material (G' < G") characterized the HPMC-C_{12} 5 wt%. Higher values of the two moduli were registered for the HPMC-C_{12} 10 wt% system, due to the higher cellulose fraction inside the gel.

Similar results were obtained in case of amplitude sweep tests performed at 37 °C for both gels, demonstrating a good stability of rheological properties at physiological conditions. Different types of composite systems were formed to obtain HPMC-C_{12}:NP (wt%) of 1:0, 1:2, 1:4 for the HPMC-C_{12} 5 wt% formulation and 1:0 and 1:1 for the HPMC-C_{12} 10 wt%. The aim of using different NPs concentrations was to verify the improvement of the final rheological properties with NPs increase. Fig. 9b and c showed the effect of the system derived from the addition of NPs on the mechanical properties. For the HPMC-C_{12} 5 wt% formulation, the storage modulus and tan(delta) increased and decreased, respectively, with increasing the nanoparticle content. This effect is the result of a higher number of polymer-nanoparticle interactions per unit volume, as reported by Appel's research group [40], in which similar results were obtained using PLA-PEG NPs. In particular, they demonstrated that the hydrophobic core of the nanoparticle is able to physically interact with the hydrophobic carbon chain C_{12} increasing the stiffness of the material. Without the presence of C_{12} the addition of NPs did not have any substantial effect on the final storage modulus. In the HPMC-C_{12} 5 wt% system the mechanical properties increased with the increase of NPs content demonstrating the improvement on mechanical properties. Indeed, the progressive decrease of tan(delta) with the increase of NPs: polymer ratio suggests a mechanical improvement towards a solid like behaviour. For the HPMC-C_{12} 10 wt% formulation with 1:0 of HPMC-C_{12}: NP (wt%) the value of storage modulus was one order of magnitude higher than that obtained for the HPMC-C_{12} 5 wt% reflecting a higher stiffness of the material. The addition of NPs in a 1:1 ratio did not have a significant influence on the elastic modulus of the gel, probably due to the low ratio used. In this case the tan (delta) remined below the value of 1, indicating a stable solid-like viscoelastic behaviour. Frequency tests were performed for the two formulations containing the highest content of NPs. Fig. 9d shows a crossover point between the storage and loss modulus and a frequency dependent response of the two moduli for both the formulations. This trend is characteristic of non-crosslinked viscoelastic materials, which present a characteristic time in the range of those investigate through the frequency sweep.

Consequently, they behave as liquid material when stimulated at low frequencies, whereas as solid if stimulated at high frequencies. These soft materials represent highly versatile systems, whose properties can be modified by changing the content of polymer or NPs. Indeed, stiffness can increase with polymer percentage, whereas the solid-like feature of the solid-viscoelastic material, can be reached by increasing NPs:polymer ratio. In this way it would be possible to modify the rheological properties of the final system depending on the final therapeutic

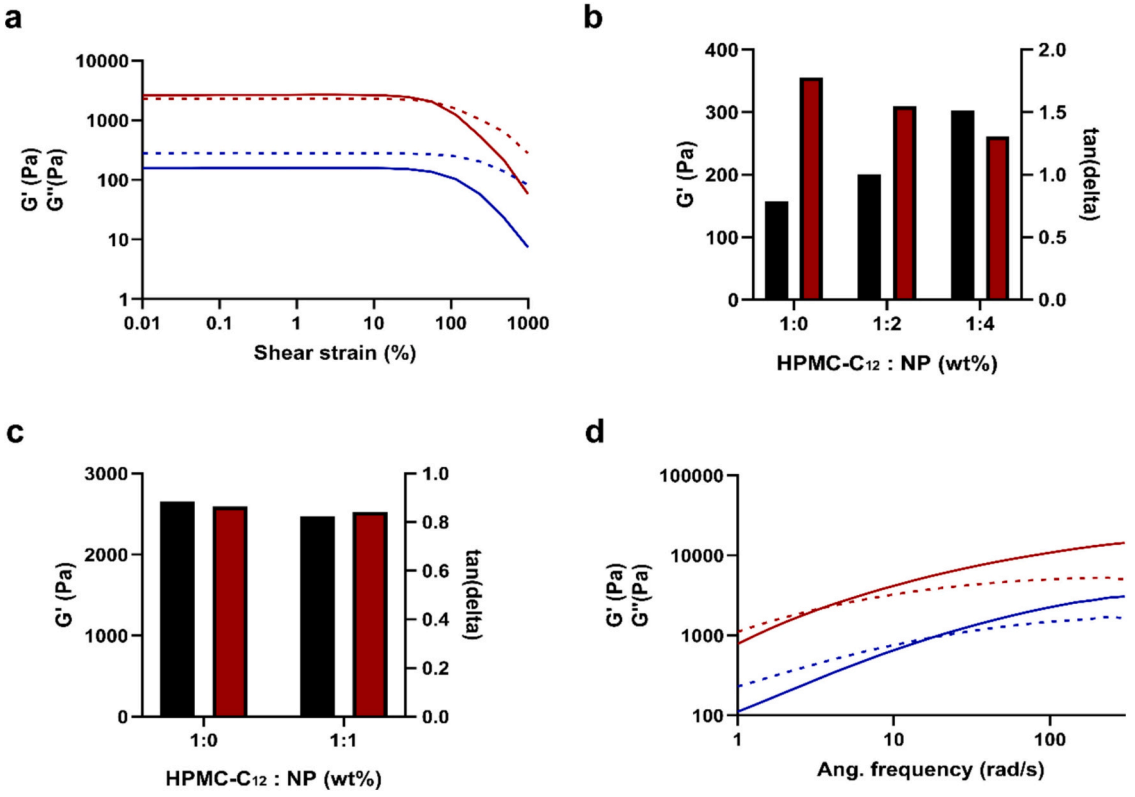

Fig. 9. (a) Amplitude sweep test: Loss modulus G″ (dashed line) and storage modulus G' (continuous line) for HPMC-C_{12} 5 wt% (blue) and HPMC-C_{12} 10 wt% (red) without NPs. (b) Amplitude sweep tests: G' (black) and tan(delta) (red) values of HPMC-C_{12} 5 wt% system at different HPMC-C_{12}:NP (wt%) ratios and (c) G' (black) and tan(delta) (red) values of HPMC-C_{12} 10 wt% system at different HPMC-C_{12}:NP (wt%) ratios. (d) frequency sweep test: G″ (dashed line) and storage modulus G' (continuous line) for HPMC-C_{12} 5 wt% with HPMC-C_{12}:NP (wt%) of 1:4 (blue) and HPMC-C_{12} 10 wt% with HPMC-C_{12}:NP (wt%) of 1:1 (red).

application and way of administration.

4. Conclusions

Innovative pH responsive nanocomposite systems incorporating pH-responsive organic NPs within a polymer network were developed starting from the controlled synthesis of ((PHEMA-*graft*-LA_{12})-*co*-PMAA)-b-PDEGMA copolymer by RAFT polymerization. pH-responsivity of NPs was guaranteed by the presence of methacrylic acid, which has an influence on intra-polymer interactions depending on its protonated or deprotonated state. The synthesis of NPs demonstrated high controlled and sustained release of mimetic drugs and a significant increase of total release for hydrophobic and slightly hydrophilic molecules decreasing the pH of external solution. In vitro test results revealed good biocompatibility of NPs and higher efficacy in decreasing cell viability over time compared to the use of only drug solution. However, cell viability measurements over 72 h should be conducted in future to confirm the higher efficiency of drug-loaded NPs compared to the pure drug administration. The inclusion of NPs inside HPCM-C_{12} polymer network resulted in improved mechanical properties of the HPMC system, confirming current literature studies. Future drug release studies will be performed from the nanocomposite material and compared to current results. The final system represents a model of co-delivery able to load therapeutic molecules of high molecular weight, such as proteins and antibodies, inside polymer network, and hydrophobic/hydrophilic drugs of low molecular weight inside the entrapped NPs. In vivo tests will be performed in future to test the ability of the presented nanocomposite system to provide a localized drug delivery after the injection and increase the release of hydrophobic drugs under specific pH conditions. The material could therefore represent a powerful tool in the development of combination therapies.

CRediT authorship contribution statement

Elisa Lacroce: Writing – original draft, Validation, Methodology. **Giuseppe Nunziata:** Writing – original draft, Methodology. **Francesca Cianniello:** Writing – review & editing, Methodology. **Emanuele Limiti:** Writing – review & editing, Methodology. **Alberto Rainer:** Writing – review & editing, Methodology. **Francesco Briatico Vangosa:** Writing – review & editing, Methodology. **Alessandro Sacchetti:** Writing – review & editing, Methodology. **Mattia Sponchioni:** Writing – review & editing, Methodology. **Filippo Rossi:** Writing – review & editing, Validation, Supervision, Conceptualization.

Declaration of competing interest

The authors declare that they have no known competing financial interests or personal relationships that could have appeared to influence the work reported in this paper.

Appendix A. Supplementary data

Supplementary data to this article can be found online at https://doi.org/10.1016/j.ijbiomac.2024.137659.

Data availability

Data will be made available on request.

References

[1] R. Dwivedi, A.K. Singh, A. Dhillon, pH-responsive drug release from dependal-M loaded polyacrylamide hydrogels, J. Sci. Adv. Mater. Devices 2 (2017) 45–50.

[2] L. Djekic, M. Martinović, V. Dobričić, B. Calija, D. Medarevic, M. Primorac, Comparison of the effect of bioadhesive polymers on stability and drug release kinetics of biocompatible hydrogels for topical application of ibuprofen, J. Pharm. Sci. 108 (2019) 1326–1333.

[3] X. Feng, C. Xing, C. Wang, Y. Tian, S. Shang, H. Liu, X. Huang, J. Jiang, Z. Song, H. Zhang, Degradable, anti-swelling, high-strength cellulosic hydrogels via salting-out and ionic coordination, Int. J. Biol. Macromol. 267 (2024) 131536.

[4] A. Pal, B.L. Vernon, M. Nikkhah, Therapeutic neovascularization promoted by injectable hydrogels, Bioact. Mater. 3 (2018) 389–400.

[5] J. Ye, X. Pan, Z. Wen, T. Wu, Y. Jin, S. Ji, X. Zhang, Y. Ma, W. Liu, C. Teng, L. Tang, W. Wei, Injectable conductive hydrogel remodeling microenvironment and mimicking neuroelectric signal transmission after spinal cord injury, J. Coll. Interf. Sci. 668 (2024) 646–657.

[6] X. Li, J. Cai, X. Duan, Y. Zhang, M. Cui, S. Wang, X. An, H. Wang, Injectable polyamide-amine dendrimer-crosslinked meloxicam-containing poly-γ-glutamic acid hydrogel for prevention of postoperative tissue adhesion through inhibiting inflammatory responses and balancing the fibrinolytic system, J. Coll. Interf. Sci. 670 (2024) 486–498.

[7] T. Yu, Y. Hu, W. He, Y. Xu, A. Zhan, K. Chen, M. Liu, X. Xiao, X. Xu, Q. Feng, L. Jiang, An injectable and self-healing hydrogel with dual physical crosslinking for in-situ bone formation, Mater. Today Bio 19 (2023) 100558.

[8] A.C. Marques, P. Cardoso Costa, S. Velho, M.H. Amaral, Injectable poloxamer hydrogels for local cancer therapy gels 9 (2023) 593.

[9] A.T. Pham, P.I. Lee, Probing the mechanisms of drug release from hydroxypropylmethyl cellulose matrices, Pharm. Res. 11 (10) (1994) 1379–1384.

[10] C. Maderuelo, A. Zarzuelo, J.M. Lanao, Critical factors in the release of drugs from sustained release hydrophilic matrices, J. Control. Release 154 (1) (2011) 2–19.

[11] A. Lu, E. Petit, Y. Wang, F. Su, S. Li, Synthesis and self-assembly of Hydroxypropyl methyl cellulose- block-poly(ε-caprolactone) copolymers as Nanocarriers of lipophilic drugs, ACS Appl. Nano Mater. 3 (2020) 4367–4375.

[12] S.H. Zainal, N.H. Mohd, N. Suhaili, F.H. Anuar, A.M. Lazim, R. Othaman, Preparation of cellulose-based hydrogel: a review, J. Mater. Res. Technol. 10 (2021) 935–952.

[13] E. Mašková, K. Kubová, B.T. Raimi-Abraham, D. Vllasaliu, E. Vohlídalová, J. Turánek, J. Mašek, Hypromellose – a traditional pharmaceutical excipient with modern applications in oral and oromucosal drug delivery, J. Control. Release 324 (2020) 695–727.

[14] H.U. Khan, S. Aziz, S. Maheen, I. Khan, M. Andleeb, H. Younis, S. Haider, A. Haider, M.S. Akhtar, S.S. Shafqat, Superporous acrylic acid and HPMC hydrogels of mefenamic acid: formulation, characterization and optimization by central composite design, Front. Bioeng. Biotechnol. 10 (2022) 1057627.

[15] M.D. Arpa, İ.M. Seçen, Ü.C. Erim, A. Hoş, N. Üstündağ Okur, Azelaic acid loaded chitosan and HPMC based hydrogels for treatment of acne: formulation, characterization, in vitro-ex vivo evaluation, Pharm. Dev. Technol. 27 (3) (2022) 268–281.

[16] X. Wang, O. Ronsin, B. Gravez, N. Farman, T. Baumberger, F. Jaisser, T. Coradin, C. Helary, Nanostructured dense collagen-polyester composite hydrogels as amphiphilic platforms for drug delivery, Adv. Sci. 8 (2021) 2004213.

[17] C. Torres-Luna, X. Fan, R. Domszy, N. Hu, N.S. Wang, A. Yang, Hydrogel-based ocular drug delivery systems for hydrophobic drugs, Eur. J. Pharm. Sci. 154 (2020) 105503.

[18] E. Larraneta, S. Stewart, M. Ervine, R. Al-Kasasbeh, R.F. Donnelly, Hydrogels for hydrophobic drug delivery. classification, synthesis and applications, J. Funct. Biomater. 9 (2018) 13.

[19] T.R. Hoare, D.S. Kohane, Hydrogels in drug delivery: Progress and challenges, Polymer 49 (2008) 1993–2007.

[20] M.A. Ward, T.K. Georgiou, Thermoresponsive polymers for biomedical applications, Polymers 3 (2011) 1215–1242.

[21] S.R. Abulateefeh, S.G. Spain, K.J. Thurecht, J.W. Aylott, W.C. Chan, M.C. Garnett, C. Alexander, Enhanced uptake of nanoparticledrug carriers via a thermoresponsive shell enhances cytotoxicity in a cancer cell line, Biomater. Sci. 1 (2013) 434–442.

[22] S.J.T. Rezaei, M.R. Nabid, H. Niknejad, A.A. Entezami, Folate-decorated thermoresponsive micelles based on star-shaped amphiphilic block copolymers for efficient intracellular release of anticancer drugs Int, J. Pharm. 437 (2021) 70–79.

[23] V. Veneruso, E. Petillo, F. Pizzetti, A. Orro, D. Comolli, M. De Paola, A. Verrillo, A. Baggiolini, S. Votano, F. Castiglione, M. Sponchioni, G. Forloni, F. Rossi, P. Veglianese, Pharmacological therapy to modulate glial cells in spinal cord injury, Adv. Mater. 36 (2024) 2307747.

[24] W.J. Geldenhuys, M.T. Khayat, J. Yun, M.A. Nayeem, Drug delivery and nanoformulations for the cardiovascular system res, Rev. Drug Deliv. 1 (2017) 32–40.

[25] Y.Q. Yang, W.J. Lin, B. Zhao, X.F. Wen, X.D. Guo, L.J. Zhang, Synthesis and physicochemical characterization of amphiphilic triblock copolymer brush containing pH-sensitive linkage for oral drug delivery, Langmuir 28 (2012) 8251–8259.

[26] X.B. Xiong, A. Falamarzian, S.M. Garg, A. Lavasanifar, Engineering of amphiphilic block copolymers for polymeric micellar drug and gene delivery, J. Control. Release 155 (2011) 248–261.

[27] E. Lacroce, F. Rossi, Polymer-based thermoresponsive hydrogels for controlled drug delivery, Expert Opin. Drug Deliv. 19 (2022) 1203–1215.

[28] C.L. Lo, K.M. Lin, G.H. Hsiue, Preparation and characterization of intelligent core-shell nanoparticles based on poly(D,l-lactide)-g-poly(N-isopropyl acrylamide-co-methacrylic acid), J. Control. Release 104 (2005) 477–488.

[29] J. Fallingborg, Intraluminal pH of the human gastrointestinal tract, Dan. Med. Bull. 46 (1999) 183–196.

[30] K. Xiao, Y. Li, J.S. Lee, W. Xiao, A.M. Gonik, R.G. Agarwal, K.S. Lam, The effect of surface charge on in vivo biodistribution of PEG-oligocholic acid based micellar nanoparticles, Biomaterials 32 (2011) 3435–3446.

[31] C. Oerlemans, W. Bult, M. Bos, G. Storm, J.F.W. Nijsen, W.E. Hennink, Polymeric micelles in anticancer therapy: targeting, imaging and triggered release, Pharm. Res. 27 (2010) 2569–2589.
[32] A. Molinelli, A. Schirato, L. Moretti, G. Della Valle, M. Maiuri, F. Rossi, Last advances on hydrogel nanoparticles composites in medicine: an overview with focus on gold nanoparticles, ChemNanoMat 10 (6) (2024) e202300584.
[33] E. Lacroce, F. Pizzetti, N.M. Barbosa Urrego, G. Nunziata, M. Masi, F. Rossi, Magnetically active Bicontinuous polymer structures for multiple controlled drug delivery, Macromol. Biosci. 24 (2024) 2400084.
[34] A.C. Yu, H. Chen, D. Chan, G. Agmon, L.M. Stapleton, A.M. Sevit, M.W. Tibbitt, J. D. Acosta, T. Zhang, P.W. Franzia, R. Langer, E.A. Appel, Scalable manufacturing of biomimetic moldable hydrogels for industrial applications, Proc. Natl. Acad. Sci. U. S. A. 113 (2016) 14255–14260.
[35] A.K. Gaharwar, N.A. Peppas, A. Khademhosseini, Nanocomposite hydrogels for biomedical applications, Biotechnol. Bioeng. 111 (2014) 441–453.
[36] S. Merino, C. Martìn, K. Kostarelos, M. Prato, E. Vàzquez, Nanocomposite hydrogels: 3D polymer À nanoparticle synergies for on-demand drug delivery, ACS Nano 9 (2015) 4686–4697.
[37] T. Jayaramudu, K. Varaprasad, R.D. Pyarasani, K.K. Reddy, A. Akbari-Fakhrabadi, V. Carrasco-Sanchez, J. Amalraj, Hydroxypropyl methylcellulose-copper nanoparticle and its nanocomposite hydrogel films for antibacterial application, Carbohydr. Polym. 254 (2021) 117302.
[38] E.L. Meany, R. Andaya, S. Tang, C.M. Kasse, R.N. Fuji, A.K. Grosskopf, A. L. d'Aquino, J.T. Bartoe, Y. Raa, A. Shelton, Z. Pederson, C. Hu, D. Leung, K. Nagapudi, S. Ubhayakar, M. Wright, C.W. Yen, E.A. Appel, Injectable polymer-nanoparticle hydrogel for the sustained intravitreal delivery of bimatoprost, Adv. Ther. 6 (2023) 2200207.
[39] A.K. Grosskopf, G.A. Roth, A.A.A. Smith, E.C. Gale, H.L. Hernandez, E.A. Appel, Injectable supramolecular polymer–nanoparticle hydrogels enhance human mesenchymal stem cell delivery, Bioeng. Transl. Med. 5 (2020) e10147.
[40] E.A. Appel, M.W. Tibbitt, M.J. Webber, B.A. Mattix, O. Veiseh, R. Langer, Self-assembled hydrogels utilizing polymer–nanoparticle interactions, Nat. Commun. 6 (2015) 6295.
[41] A.K. Grosskopf, O.A. Saouaf, H.L. Hernandez, E.A. Appel, Gelation and yielding behavior of polymer-nanoparticle hydrogels, J. Polym. Sci. 59 (2021) 2854–2866.
[42] G.A. Roth, O.M. Saouaf, A.A.A. Smith, E.C. Gale, M. Alcantara Hernandez, J. Idoyaga, E.A. Appel, Prolonged codelivery of hemagglutinin and a TLR7/8 agonist in a supramolecular polymer–nanoparticle hydrogel enhances potency and breadth of influenza vaccination, ACS Biomater Sci. Eng. 7 (5) (2021) 1889–1899.
[43] A.N. Steele, L.M. Stapleton, J.M. Farry, H.J. Lucian, M.J. Paulsen, A. Eskandari, C. E. Hironaka, A.D. Thakore, H. Wang, A.C. Yu, D. Chan, E.A. Appel, Y.J. Woo, A biocompatible therapeutic catheter-deliverable hydrogel for in situ tissue engineering, Adv. Healthc. Mater. 8 (5) (2019) 1801147.
[44] V. Makker, N. Colombo, A. Casado Herráez, A.D. Santin, E. Colomba, D.S. Miller, K. Fujiwara, S. Pignata, S. Baron-Hay, I. Ray-Coquard, R. Shapira-Frommer, K. Ushijima, J. Sakata, K. Yonemori, Y.M. Kim, E.M. Guerra, U.A. Sanli, M. M. McCormack, A.D. Smith, S. Keefe, S. Bird, L. Dutta, R.J. Orlowski, D. Lorusso, Study 309–KEYNOTE-775 investigators. Lenvatinib plus Pembrolizumab for advanced endometrial Cancer, New Engl. J. Med. 386 (2022) 437–448.
[45] L. Paz-Ares, M. Dvorkin, Y. Chen, N. Reinmuth, K. Hotta, D. Trukhin, G. Statsenko, M.J. Hochmair, M. Özgüroğlu, J.H. Ji, O. Voitko, A. Poltoratskiy, S. Ponce, F. Verderame, L. Havel, I. Bondarenko, A. Kazarnowicz, G. Losonczy, N.V. Conev, J. Armstrong, N. Byrne, N. Shire, H. Jiang, G.J. Wa, Durvalumab plus platinum-etoposide versus platinum-etoposide in first-line treatment of extensive-stage small-cell lung cancer (CASPIAN): a randomised, controlled, open-label, phase 3 trial, Lancet 394 (2019) 1929–1939.
[46] Y. Doki, J.A. Ajani, K. Kato, J. Xu, L. Wyrwicz, S. Motoyama, T. Ogata, H. Kawakami, C.H. Hsu, A. Adenis, F. El Hajbi, M. Di Bartolomeo, M.I. Braghiroli, E. Holtved, S.A. Ostoich, H.R. Kim, M. Ueno, W. Mansoor, W.C. Yang, T. Liu, J. Bridgewater, T. Makino, I. Xynos, X. Liu, M. Lei, K. Kondo, A. Patel, J. Gricar, I. Chau, Y. Kitagawa, Nivolumab combination therapy in advanced esophageal squamous-cell carcinoma, New Engl. J. Med. 386 (2022) 449–462.
[47] J. Watanabe, K. Muro, K. Shitara, K. Yamazaki, M. Shiozawa, H. Ohori, A. Takashima, M. Yokota, A. Makiyama, N. Akazawa, H. Ojima, Y. Yuasa, K. Miwa, H. Yasui, E. Oki, T. Sato, T. Naitoh, Y. Komatsu, T. Kato, M. Hihara, J. Soeda, T. Misumi, K. Yamamoto, K. Akagi, A. Ochiai, H. Uetake, K. Tsuchihara, T. P. Yoshino, Anitumumab vs bevacizumab added to standard first-line chemotherapy and overall survival among patients with RAS wild-type, left-sided metastatic colorectal cancer: a randomized clinical trial, JAMA 329 (2023) 1271–1282.
[48] M.G. Fakih, L. Salvatore, T. Esaki, D.P. Modest, D.P. Lopez-Bravo, J. Taieb, M. V. Karamouzis, E. Ruiz-Garcia, T.W. Kim, Y. Kuboki, F. Meriggi, D. Cunningham, K. H. Yeh, E. Chan, J. Chao, Y. Saportas, Q. Tran, C. Cremolini, F. Pietrantonio, Sotorasib plus Panitumumab in refractory colorectal Cancer with mutated KRAS G12C, New Engl. J. Med. 389 (2023) 2125–2139.
[49] T.K. Choueiri, T. Powles, L. Albiges, M. Burotto, C. Szczylik, B. Zurawski, E. Yanez Ruiz, M. Maruzzo, A. Suarez Zaizar, L.E. Fein, F.A. Schutz, D.Y.C. Heng, F. Wang, F. Mataveli, Y.L. Chang, M. van Kooten Losio, C. Suarez, R.J. Motzer, Cabozantinib plus Nivolumab and Ipilimumab in Renal-Cell Carcinoma, New Engl. J. Med. 388 (2023) 1767–1778.
[50] H. Luo, J. Lu, Y. Bai, T. Mao, J. Wang, Q. Fan, Y. Zhang, K. Zhao, Z. Chen, S. Gao, J. Li, Z. Fu, K. Gu, Z. Liu, L. Wu, X. Zhang, J. Feng, Z. Niu, Y. Ba, H. Zhang, Y. Liu, L. Zhang, X. Min, J. Huang, Y. Cheng, D. Wang, Y. Shen, Q. Yang, J. Zou, R.H. Xu, Effect of Camrelizumab vs placebo added to chemotherapy on survival and progression-free survival in patients with advanced or metastatic esophageal squamous cell carcinoma: the ESCORT-1st randomized clinical trial, JAMA 326 (2021) 916–925.
[51] M. Attal, P.G. Richardson, S.V. Rajkumar, J. San-Miguel, M. Beksac, I. Spicka, X. Leleu, F. Schjesvold, P. Moreau, M.A. Dimopoulos, J.S. Huang, J. Minarik, M. Cavo, H.M. Prince, S. Macé, K.P. Corzo, F. Campana, S. Le-Guennec, F. Dubin, K. C. Anderson, Isatuximab plus pomalidomide and low-dose dexamethasone versus pomalidomide and low-dose dexamethasone in patients with relapsed and refractory multiple myeloma (ICARIA-MM): a randomised, multicentre, open-label, phase 3 study, Lancet 394 (2019) 2096–2107.
[52] S.Z. Usmani, H. Quach, M.V. Mateos, O. Landgren, X. Leleu, D. Siegel, K. Weisel, M. Gavriatopoulou, A. Oriol, N. Rabin, A. Nooka, M. Qi, M. Beksac, A. Jakubowiak, B. Ding, A. Zahlten-Kumeli, A. Yusuf, M. Dimopoulos, Carfilzomib, dexamethasone, and daratumumab versus carfilzomib and dexamethasone for patients with relapsed or refractory multiple myeloma (CANDOR): updated outcomes from a randomised, multicentre, open-label, phase 3 study, Lancet Oncol. 23 (2022) 65–76.
[53] A. Kawazoe, T. Ando, H. Hosaka, J. Fujita, K. Koeda, K. Nishikawa, K. Amagai, K. Fujitani, K. Ogata, K. Watanabe, Y. Yamamoto, K. Shitara, Safety and activity of trifluridine/tipiracil and ramucirumab in previously treated advanced gastric cancer: an open-label, single-arm, phase 2 trial, lancet, Gastroenterol. Hepatol. 6 (2021) 209–217.
[54] Y.Y. Janjigan, K. Shitara, M. Moehler, M. Garrido, P. Salman, L. Shen, L. Wyrwicz, K. Yamaguchi, T. Skoczylas, A. Campos Bragagnoli, T. Liu, M. Schenker, P. Yanez, M. Tehfe, R. Kowalyszyn, M.V. Karamouzis, R. Bruges, T. Zander, R. Pazo-Cid, E. Hitre, K. Feeney, J.M. Cleary, V. Poulart, D. Cullen, M. Lei, H. Xiao, K. Kondo, M. Li, J.A. Ajani, First-line nivolumab plus chemotherapy versus chemotherapy alone for advanced gastric, gastro-oesophageal junction, and oesophageal adenocarcinoma (CheckMate 649): a randomised, open-label, phase 3 trial, Lancet 398 (2021) 27–40.
[55] U. Sahin, O. Tureci, G. Manikhas, F. Lordick, A. Rusyn, I. Vynnychenko, A. Dudov, I. Bazin, I. Bondarenko, B. Melichar, K. Dhaene, K. Wiechen, C. Huber, D. Maurus, A. Arozullah, J.W. Park, M. Schuler, S.E. Al-Batran, FAST: a randomised phase II study of zolbetuximab (IMAB362) plus EOX versus EOX alone for first-line treatment of advanced CLDN18.2-positive gastric and gastro-oesophageal adenocarcinoma, Ann. Oncol. 32 (2021) 609–619.
[56] Y. Zhang, J. Li, M. Lang, X. Tang, L. Li, X. Shen, Folate-functionalized nanoparticles for controlled 5-fluorouracil delivery, J. Coll. Interf. Sci. 354 (2011) 202–209.
[57] U. Capasso Palmiero, A. Agostini, E. Lattuada, S. Gatti, J. Singh, C.T. Canova, S. Buzzaccaro, D. Moscatelli, Use of RAFT macro-surfmers for the synthesis of transparent aqueous colloids with tunable interactions, Soft Matter 13 (2017) 6439–6449.
[58] S. Hemaiswarya, M. Doble, Combination of phenylpropanoids with 5-fluorouracil as anti-cancer agents against human cervical cancer (HeLa) cell line, Phytomedicine 20 (2013) 151–158.
[59] B. Özkahraman, I. Acar, G. Güçlü, Synthesis of N-vinylcaprolactam and methacrylic acid based hydrogels and investigation of drug release characteristics, Polym. Bull. 80 (2023) 5149–5181.
[60] M. Sponchioni, U.C. Palmiero, D. Moscatelli, HPMA-PEG Surfmers and their use in stabilizing fully biodegradable polymer nanoparticles, Macromol. Chem. Phys. 218 (2017) 1–12.
[61] N. Rapoport, Physical stimuli-responsive polymeric micelles for anti-cancer drug delivery, Prog. Polym. Sci. 32 (2007) 962–990.
[62] L. Jongpaiboonkit, Z. Zhou, X. Ni, Y.Z. Wang, J. Li, Self-association and micelle formation of biodegradable poly(ethylene glycol)-poly(L-lactic acid) amphiphilic di-block co-polymers, J. Biomater. Sci. Polym. Ed. 17 (2006) 747–763.
[63] S. Holappa, M. Karesoja, J. Shan, H. Tenhu, Solution properties of linear and branched block copolymers consisting of acidic and PEO blocks, Macromolecules 35 (2002) 4733–4738.
[64] S.F. Medeiros, M.V. Lopes, B. Rossi-Bergmann, M.I. Ré, A.M. Santos, Synthesis and characterization of poly(N-vinylcaprolactam)-based spray-dried microparticles exhibiting temperature and pH-sensitive properties for controlled release of ketoprofen, Drug Dev. Ind. Pharm. 43 (2017) 1519–1529.
[65] R. Liu, Y. Tao, Y. Zhu, M. Chen, C. Yang, X. Liu, Synthesis of double-hydrophilic poly(methylacrylic acid)-poly(ethylene glycol)-poly(methylacrylic acid) triblock copolymers and their micelle formation, Polym. Int. 60 (2011) 327–332.
[66] A.M. Lowman, N.A. Peppas, Molecular analysis of interpolymer complexation in graft copolymer networks, Polymer 41 (2000) 73–80.
[67] Y. Zheng, L. Wang, L. Lu, Q. Wang, B.C. Benicewicz, pH and thermal dual-responsive nanoparticles for controlled drug delivery with high loading content, ACS Omega 2 (7) (2017) 3399–3405.
[68] C.C. Lin, A.T. Metters, Hydrogels in controlled release formulations: network design and mathematical modeling, Adv. Drug Deliv. Rev. 58 (2006) 1379–1408.
[69] P.L. Ritger, N.A. Peppas, A simple equation for description of solute release I. Fickian and non-Fickian release from non-swellable devices in the form of slabs, spheres, cylinders or discs, J. Control. Release 5 (1987) 23–36.
[70] Remington's Pharmaceutical Sciences, 15th edition, Mack Publishing Co., Easton, PA, 1976.
[71] M.A. Khan, A.K. Azad, M. Safdar, A. Nawaz, M. Akhlaq, P. Paul, M.K. Hossain, M. H. Rahman, R.S. Baty, A.F. El-kott, M. Kamel, S.G. Bungau, M.M. Abdel-Daim, Synthesis and characterization of acrylamide/acrylic acid co-polymers and glutaraldehyde crosslinked pH-sensitive hydrogels, Gels 8 (1) (2022) 47.
[72] B.K. Kwon, E.B. Okon, W. Plunet, D. Baptiste, K. Fouad, J. Hillyer, L.C. Weaver, M. G. Fehlings, W. Tetzlaff, A systematic review of directly applied biologic therapies for acute spinal cord injury, J. Neurotrauma 28 (2011) 1589–1610.

[73] M.S. Toftdal, N.P. Christensen, F.B. Kadumudi, A. Dolatshahi-Pirouz, L.G. Grunnet, M. Chen, Mechanically reinforced hydrogel vehicle delivering angiogenic factor for beta cell therapy, J. Coll. Interf. Sci. 667 (2024) 54–63.
[74] K. Vulic, M.S. Shoichet, Tunable growth factor delivery from injectable hydrogels for tissue engineering, J. Am. Chem. Soc. 134 (2012) 882–885.
[75] A. Lu, E. Petit, Y.Z. Wang, F. Su, S. Li, Synthesis and self-assembly of hydroxypropyl methyl cellulose- block-poly(ε-caprolactone) copolymers as nanocarriers of lipophilic drugs, ACS Appl. Nano Mater. 3 (2020) 4367–4375.
[76] C. Chang, B. Duan, J. Cai, L. Zhang, Superabsorbent hydrogels based on cellulose for smart swelling and controllable delivery, Eur. Polym. J. 46 (2010) 92–100.
[77] L. Jiang, X. Huang, C. Tian, Y. Zhong, M. Yan, C. Miao, T. Wu, X. Zhou, Preparation and characterization of porous cellulose acetate nanofiber hydrogels gels 9 (2023) 484.